Journal of Non –Oxide Glasses Vol. 11, No. 2, April - June 2019, p. 19 - 26

NUMERICAL OPTIMIZATION FOR AlGaN/GaN HEMTs INCLUDING POLARIZATION COULOMB FIELD SCATTERING

R. YAHYAZADEH[*], Z. HASHEMPOUR
Department of Physics, Khoy Branch, Islamic Azad University, Khoy, Iran

A numerical model for I–V characteristics of AlGaN/GaN-based high electron mobility transistors (HEMTs) has been developed that is capable to predict accurately the effects of self-heating, polarization Coulomb Field Scattering(PCF), multi sub-band on drain-source current and extrinsic transconductance. Salient features of the model are incorporated of fully and partially occupied sub-bands in the interface quantum well, combined with a self-consistent solution of the Schrodinger and Poisson equations. In addition, to develop the model, accurate two-dimensional electron gas mobility and modified wave function in barrier AlGaN have been used. It is found that the variation of the drain-source current, extrinsic and transconductance originates from the polarization Coulomb field scattering, multi sub-band effect and self-heating is more significant in the saturation region. The calculated model results are in good agreement with existing experimental data.

(Received March 3, 2019; Accepted April 10, 2019)

Keywords: PCF scattering, Self-heating, Multi sub-band, NDC

1. Introduction

AlGaN/GaN heterostructure field-effect transistors (HFETs) have been interested in RF applications because of their outstanding high-frequency and high-power performance [1–3]. Linearity is one of the most crucial figures of merit for the application of power amplifiers. For improving the device linearity, advanced device structures or epitaxial structure engineerings, such as field plate, nonlinear polarization dielectric, double-channel, and optimized barrier or cap layer thickness, has been explored [4–7]. Polarization Coulomb field (PCF) scattering, which stems from the non-uniform distribution of the polarization charges at the AlGaN/GaN interface, is a particular scattering mechanism in AlGaN/GaN HFETs. It has been reported that PCF scattering can affect the electron mobility, parasitic source access resistance (R_S), device and extrinsic transconductance (g'_m) [8–9]. Besides, III–V nitride-based HEMTs simulations show that the Polarization Coulomb Field Scattering plays a very important role in limiting the device performance, especially saturation region [10,11]. However, the high power dissipation of AlGaN/GaN HEMTs operating at large biases may result in high junction temperature and enhance the phonon scattering causing a drop in carrier mobility. This effect has been reported to be of great influence on the static current characteristics and is commonly referred to as self-heating. The evidence of such an effect is a negative slope of drain current I_{DS} versus drain voltage V_{DS} [12]. More recently, the drain-source current of III nitride-based HEMT has been modeled by several groups analytically, numerically or analytical-numerically [12-14,38]. It is important to investigate systematically the dependence of AlGaN–GaN HEMT performance on the Polarization Coulomb Field Scattering, self-heating and multi sub-band with including different physical parameters. In this paper, we report our results on the effects of Polarization Coulomb Field Scattering on a small signal parameter such as drain-source current and extrinsic transconductance with including self-heating and multi sub-band. The drain-source current of these transistors was previously calculated without including PCF scattering and multi sub-band effect [12]. In the present work, a new numerical model for total resistance, drain-source current and extrinsic transconductance is presented. That is capable of determining effects of self-heating, PCF scattering and multi sub-band on the drain-source current. This is achieved by (i) using a self-

[*] Corresponding author: yahyazadehs@gmail.com

consistent solution of the Schrödinger and Poisson equations in order to obtain both two-dimensional electron gas density, wave function, Fermi level (E_{Fi}) specified relative to the bottom of a triangular well, (ii) take into account the modified wave function in the AlGaN barrier, (iii) take into account the self-heating, (iv) take into account the occupancy of the various sub-bands, the intrasubband, and intersubband coupling coefficientsH_{mn}. The fringing-field effect can be ignored in the present numerical model.

2. Materials and methods

In order to obtain accurate values for the Fermi energy, the energies of quantized levels within the 2DEG, the occupancy of the various sub-bands, the intrasubband and intersubband coupling coefficients, potential profiles, wave function and the sheet carrier concentration for the 2DEG in AlGaN/GaN heterostructures; both the Schrödinger and Poisson equations must be solved self-consistently. This has been achieved by solving Schrödinger's equation and simultaneously taking into account the electrostatic potential obtained from Poisson's equation, as well as the image and exchange-correlation potentials using Numerov's numerical method. In the self-consistent calculation, the nonlinear formalism of the polarization–induced field as a function of Al mole fraction in *AlGaN / GaN* heterostructures has been assumed, as well as taking in to account all fully and partially occupied sub-bands within the interface 2DEG potential well [13,15]. Using such an approach, it is possible to calculate the 2D-electron mobility taking into account the combined contributions from each of the individual electron scattering mechanisms [16]. In the FET model, the x-direction is along the 2DEG channel and the z-direction is along the growth direction. Knowing the electron energy in any sub-bandE_i , the 2DEG density n_{2D} , and the Fermi energy can be calculated [12, 16, 18, and 19]. The Quantum correction for the effective width of the 2-DEG($\Delta d_{2DEG} = 1/n_{2D} \int z n_{2D}(z) dz$) at a different temperature is given by [20]:

$$\Delta d_{2DEG} = 5.6 \times 10^{-9} T + 4.7 \times 10^{-8} \tag{1}$$

The additional polarization charge $\Delta\sigma$ in the gate region can be calculated as following relation [21, 22, and 23]:

$$\Delta\sigma = \frac{e_{33}^2}{C_{33}} \Delta E_z^{AlGaN} \tag{2}$$

Here, e_{33} ,C_{33} and d_{AlGaN} are the piezoelectric coefficients, the elastic stiffness tensor and barrier thickness of AlGaN, respectively, $\Delta E_z^{AlGaN} = \left(V_{GS} - V_{CH}(x)\right)/d_{AlGaN}$ is the vertical direction electric field across the AlGaN barrier layer. ΔE_z^{AlGaN} and $\Delta\sigma$ under the various gate-source voltage V_{GS} and channel potential V_{CH} are calculated using Eq. (3).The energy-dependent momentum relaxation rate $1/\tau_{PCF}$ for PCF scattering can be written as [21,24]:

$$\frac{1}{\tau_{PCF}} = \frac{Am^*}{2\pi\hbar^3} \int_0^{\pi} \left[\frac{M_{k-k'}}{S(q,T_e)}\right] (1 - cos\theta) d\theta \tag{3}$$

where A is the 2-D normalization constant that converts the scattering rate per area and θ is the scattering angle between initial state k and final state k'. $S(q,T_e)$ is the screening function to reflect the screening effect and $M_{k-k'}$ is the matrix element (depend on the wave function) for the transition from initial state k to the final state k' [24]. The wave function, although being very practical for most of the relevant mobility related calculation, has the drawback of being zero in the barrier region. This is equivalent to consider the barrier as infinitely high. However, alloy scattering is a mobility-limiting mechanism intrinsically related to the penetration wave function in the barrier region. This can be overcome by using a modified Fang-Howard wave function [25].

Besides PCF scattering, the other main scattering mechanisms are polar-optical-phonon (POP) scattering, piezoelectric (PE) scattering, alloy scattering (Alloy), dislocation scattering (DIS),acoustic-phonon (AP), and interface roughness (IFR) scattering[28-31,16].The momentum relaxation time τ_{IFR}, τ_{DIS}, τ_{POP}, τ_{Alloy} , $\tau_{AP}$and τ_{PE} can be calculated using the pre-existing calculation formula[11,26]. By Matthiessen's rule, R_C and R_D can be written as:

$$R_{CH} = R_G = \frac{m^* L_G}{n_{2D} e^2 W_G}\left(\frac{1}{\tau_{PCF}} + \frac{1}{\tau_{POP}^G} + \frac{1}{\tau_{AP}^G} + \frac{1}{\tau_{IFR}^G} + \frac{1}{\tau_{DIS}^G} + \frac{1}{\tau_{Alloy}^G}\right) \quad (4)$$

$$R_F = \frac{m^*(L_{GS}+L_{GD})}{n_{2D0} e^2 W_G}\left(\frac{1}{\tau_{PCF}} + \frac{1}{\tau_{POP}^F} + \frac{1}{\tau_{AP}^F} + \frac{1}{\tau_{IFR}^F} + \frac{1}{\tau_{DIS}^F} + \frac{1}{\tau_{Alloy}^F}\right) \quad (5)$$

$$R_{total} = R_G + R_F + 2R_C \text{ , } R_F = R_S + R_D \text{ , } R_{CH} = R_G \quad (6)$$

The contact resistance of RC is a constant and the R_S is different value during the measurement. As a result, R_S is determined by the scattering mechanisms for the electrons in the gate-source channel [27, 28]. In order to obtain accurate values for mobility, the nonlinear formalism of the polarization–induced field as a function of Al mole fraction in AlmGa1-mN/GaN HEMTs have been assumed, as well as taking into account intersubband coupling coefficients H_{mn} and all fully and partially–occupied sub-bands within the interface 2DEG potential well. From the definition of the drift mobility we obtain [28-30]:

$$\boldsymbol{\mu_{2DEG}(T,E) = \frac{e}{m^*}\langle \tau_{total}(T,E)\rangle} \quad (7)$$

where τ_{total} are the total relaxation times associated with PCF scattering and the other main scattering mechanisms so that these relaxation times have been calculated using the methods described in Refs [28-31,16]. Also, the different scattering rates can be separated into two types: (i) elastic scattering due to acoustic and piezoelectric phonons, ionized impurities and interface roughness, etc., and (ii) inelastic scattering due to polar optical phonons. In order to take into consideration all scattering mechanisms in the mobility calculation, it is necessary to include all such mechanism in the linearized Boltzmann equation and to solve it numerically using an iterative technique [9]. It should be noted that in the linearized Boltzmann equation, $\Phi(E,T)$ is the perturbation function so that to obtain the $\Phi(E,T)$ needs to take into account the contribution of all occupied sub-bands by means of following relation [16]:

$$\frac{1}{\Phi(E,T)} = \sum_m \sum_n \frac{n_m}{n_{2DEG}} \frac{1}{\Phi_{mn}} \quad (8)$$

Equation (3) indicated that all occupied states contribute to the total mobility of the two-dimensional electron gases. This equation also shows that the contribution of each sub-band depends on its occupation number (that is relative concentration n_m/n_{2DEG})such that the most significant contribution comes from the first sub-band, which has the highest occupation number. Using such an approach, it is possible to calculate the 2D-electron mobility taking into account the combined contributions from each of the individual electron scattering mechanisms

The drain-source current is given by the following relation [14, 32, and 33]:

$$I_{DS} = \begin{cases} Wqv(T,m,E)n_{2D}(V_{GS},x,m.T) - qD(T,E)\frac{dn_{2D}(V_{GS},x,m,T)}{dx} & \textit{Linear region} \\ Wqv_{sat}(T,m)n_{2D}(V_{GS},x,m,T) - qD(T)\frac{dn_{2D}(V_{GS},x,m.T)}{dx} & \textit{saturation region} \end{cases} \quad (9)$$

where the first term is the drift current and the second represents the diffusion current, W is the gate width, E is the electric field, $v(T,m,E)$ is the electron drift velocity and $D(T,m)$ is the electron diffusion constant which can be assumed to be related to the mobility via the classical Einstein relation for low field given by $D(T,m) = k_B T\mu(T)/q$ However, in order to solve Eq. (17), it is necessary to invoke the following, boundary condition at the source and drain ends of the channel region:

$$V_{ch}(0) = I_{DS} \times (R_S + R_C)$$

$$V_{ch}(L_{SG} + L_G + L_{GD}) = V_{DS} - I_{DS} \times (R_D + R_C) \tag{10}$$

As evident from the equations, the transport parameters of the 2DEG are dependent on temperature. However, the temperature of the device is different from the electron gas channel temperature because of self-heating effects. During the calculation, the self-heating effect has been taken into account as follows. The temperature difference between the channel and the bottom of the substrate ($\Delta T = T_{ch} - T_{sub}$) is [34]:

$$\frac{\Delta T}{T_{sub}} = \frac{\left(1-(P_{diss}/4P_0)^4\right)}{(1-P_{diss}/4P_0)^4} \tag{11}$$

where T_{ch} is the channel temperature and T_{sub} is the temperature of the substrate bottom.P_0 is referred to as a characterization quality with the dimension of power

$$P_0 = \frac{\pi K(T_{sub})WT_{sub}}{ln(8t_{sub}/\pi L_G)} \tag{12}$$

where $P_{diss} = I_{DS}V_{DS}$ is the power dissipation, t_{sub} is the thickness of the substrate, L_G is the length of the gate and $K(T_{sub})$ is the thermal conductivity. The initial value of V_{DS} is evaluated for a given I_{DS}, thenΔT and other parameters at this temperature are calculated from Eqs. (17-20). Repeating similar steps for a certain range of I_{DS}, the corresponding values of V_{DS} and the I-V characteristics of the device are achieved [12,35]. The 2D transport model analysis steps as shown in Fig. 1. Knowing the current-voltage characteristics one can find the small signal parameters such as the extrinsic transconductance, g'_mdrain conductance, g_d and the gate-to-source capacitance, C_{GS} . The transconductance and drain conductance can be defined by differentiating of I_{DS} with respect to V_{GS} and V_{DS} keeping$V_{DS}$and V_{GS}constant, respectively.

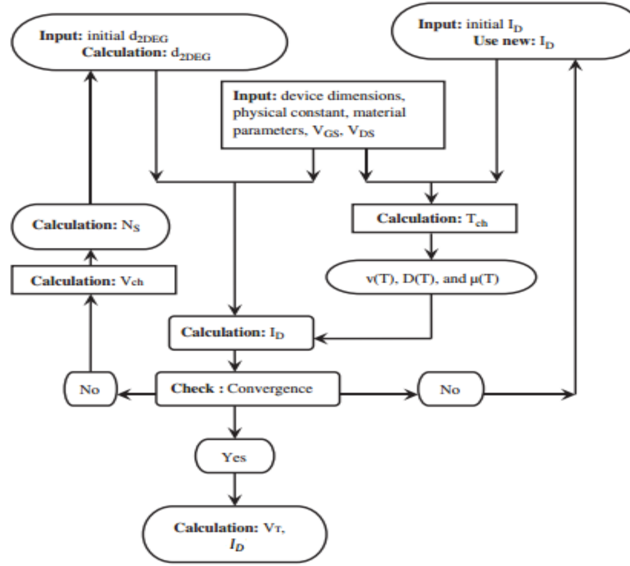

Fig. 1. The 2D transport model analysis steps.

3. Results and discussion

To assess the validity of the numerical model for the negative differential conductivity of quantum well a comparative study has been undertaken to compare theoretically obtained, n_{2D}, R_{total}, I_{DS}, g'_m, andf_T and curves with experimental results. The experimental results, material and device details and all other material parameters have been taken from Refs. 10,17, 20, 36 and 37 for $Al_mGa_{m-1}N/GaN$ ($m = 0.24$ and 0.15) HEMTs. Fig. 2 show that as the L_G increases, the 2DEG density decrease and the threshold voltage shifts towards increasingly negative values. The large values of n_{2D} are attributed to the presence of polarization induced charges in AlGaN/GaN HEMTs, which have been incorporated accurately in the proposed model. The slope of the $n_{2D} - V_{GS}$ curves corresponds to the capacitance of the structure, which is related directly to the separation between the gate and the 2DEG, i.e. the thickness of AlGaN layer. As the $L_G$decrease, the slope of the $n_{2D} - V_{GS}$ curves beyond the threshold slightly increases. This is due to the fact that gate capacitance decreases as L_G decreases. For $L_G = 4\mu m$, the slope is obtained as $1.9551012 cm^{-2}V^{-1}$, whereas for $L_G = 16\mu m$, the slope decreases to $1.81012 cm^{-2}V^{-1}$. Thus a lower value of L_G is desirable to achieve a high value of 2- DEG density and lower values of gate capacitance. The wave function under differentn_{2D}, can be calculated from the self-consistent solution of the Schrödinger and Poisson equations and modified Fang-Howard wave function, as shown in Fig. 3. It is apparent wave function is closely relevant with n_{2D}. The larger n_{2D}, of 2DEG electrons and modified Fang-Howard wave function (inset of Fig. 3) is closer the AlGaN/GaN interface. Hence wave function depends onn_{2D}. The calculated $R_{total}$for devices were shown in Fig. 4 Firstly, there is a distinct difference between the experimental data and calculated R_{total} excluding PCF scattering and multi sub-band effect. This means PCF scattering and multi sub-band effect is not ignorable in AlGaN/GaN HEMTs. However, the increase in V_{GS} (here, the increase of V_{GS}means that the V_{GS} is changed from -3 V to 0 V) and, thus, the decrease in the electric potential in the channel under the gate induces the decrease/increase in the negative/positive $\Delta\sigma$, according to Eq. (2). So that, PCF scattering gets weaker with the increase in V_{GS}, inducing a decrease in R_{total}. As a result, as $V_{GS}$is increased, $\Delta\sigma$ decreases and PCF scattering becomes weaker. On the other hand, it is apparent that both $\Delta E_z^{AlGaN}$and $\Delta\sigma$ are decreased with decreased V_{CH} . For the sample HEMTs, a small V_{CH} means a small V_{DS}. Therefore, the smaller the V_{DS} (V_{CH}) is the smaller the ΔE_z^{AlGaN} and $\Delta\sigma$. Thus, the PCF scattering becomes weaker with the decrease of V_{DS}. In consequence, both the increase of $V_{GS}$and the decrease of

V_{DS}can weaken PCF scattering. For $V_{DS} > 5V$ (V_{GS} around +1V), electron (in the gate–source channel) drift velocity is more than $1.5 \times 10^6 m/s$ when I_{DS} is increased to around $37mA$. The electron and POP temperatures start to increase, inducing an increase in $R_{total}$and a decrease in I_{DS}, g'_m, as shown in Figs. 4,5 and 6. The effects of Polarization Coulomb Field Scattering on drain-source current and extrinsic transconductance with including self-heating and multi sub-band was shown in Figs. 5, 6. It is found that the variation of the drain-source current and total resistance originates from the polarization Coulomb field (PCF) scattering and multi sub-band effect are more significant so that negative differential conductivity(NDC) in Fig. 6 originate from self-healing, PCF scattering and multi sub-band are ~%70, %20, %10 respectively. The calculated model results are in very good agreement with existing experimental data. The extrinsic transconductance g'_m, is closely related to R_S and g_m (or dependent of R_{total}), as a result R_S and R_{total} are greatly influenced by PCF scattering, multi sub-band, and self-heating respectively. As shown in the figure there is a good agreement between the experimental data and our model calculations.

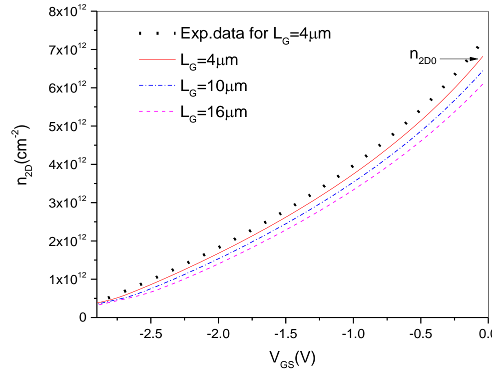

Fig. 2. The 2DEG density (n_{2D}) verse V_{GS} for $Al_{0.24}Ga_{0.76}N/GaN$ HEMTs with different gate length in comparison with experimental data [36].

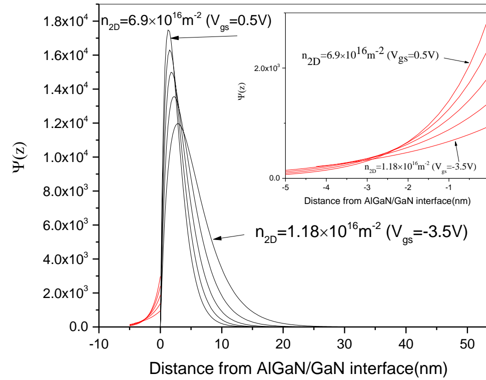

Fig. 3. The electron wave function ψ(z) as a function of the distance from AlGaN/GaN Interface under different n_{2D} (heren_{2D}corresponds to the electron density under the gate region as a function of gate bias).

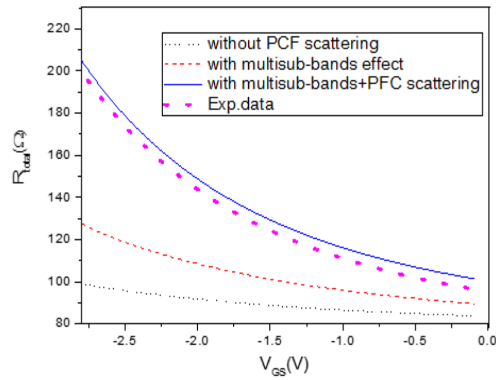

Fig. 4. Source-drain channel resistance without PCF scattering effect (dot line), with multi sub-band effect (dashed line) and with all effect (solid line) in comparison with experimental data for $Al_{0.24}Ga_{0.76}N/GaN$ HEMTs [36].

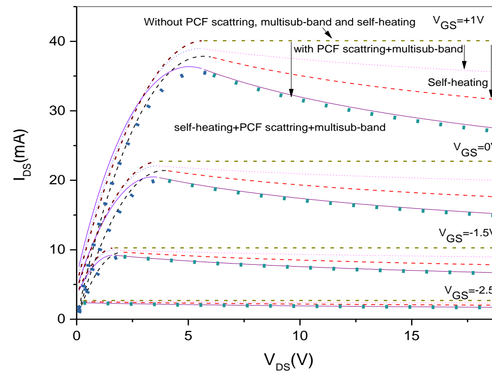

Fig. 5. Drain current versus source-drain voltage for the $Al_{0.24}Ga_{0.76}N/GaN$ HEMTs, including PCF scattering and multi sub-band (dot line), self- heating (dashed line) and with including all effect (solid line) in comparison with experimental data [10].

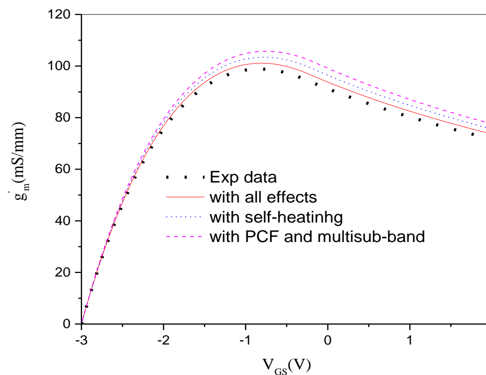

Fig. 6. Extrinsic transconductance versus gate-source voltage for the $Al_{0.24}Ga_{0.76}N/GaN$ HEMTs, including PCF scattering and multi sub-band (dot line) , self- heating (dashed line) and with including all effect (solid line) at $V_{DS} = 10V$ in comparison with experimental data [28].

4. Conclusions

In this paper, an accurate numerical model for negative differential conductivity of quantum well has been developed for the AlGaN/GaN-based HEMTs. This model is able to accurately predict the dependence of drain-source current and extrinsic transconductance on the total resistance, polarization Coulomb field (PCF) scattering, multi sub-band, and self-heating. From the results, it is apparent that for $V_{DS} > 4V$, electron drift velocity and I_{DS} is increased as results the electron density and POP scattering start to increase, inducing an increase in R_{total} and a decrease in I_{DS} and g'_m . In addition, negative differential conductivity(NDC) originate from self-healing, PCF scattering and multi sub-band are ~%70, %20, %10 respectively. The results of our study are in good agreement with experimental data published in the literature.

References

[1] A. D. Latorre-Rey, F. F. M. Sabatti, J. D. Albrecht, M. Saraniti, Appl. Phys. Lett. **111**, 013506 (2017).
[2] J. Ma, E. Matioli, Slanted IEEE Electron Device Lett. **38**, 1305 (2017).
[3] G. Tang et al., IEEE Electron Device Lett. **38**, 1282 (2017).
[4] M. Blaho et al., Annealing, Appl. Phys. Lett. **111**, 033506 (2017).
[5] K. Zhang et al., IEEE Electron Device Lett. **38**, 615 (2017).
[6] H. Chiu et al., IEEE Trans. Electron Devices. **64**, 4065 (2017).
[7] S. Sun et al., Appl. Phys. Lett. **108**, 013507 (2016).
[8] D. F. Brown et al., IEEE Electron Device Lett. **38**, 1445 (2017).
[9] L. Yang et al., IEEE Electron Device Lett. **38**, 1563 (2017).
[10] P. Cui et al., IEEE Trans. Electron Devices. **64**, 1038 (2017).
[11] P. Cui et al., J. Appl. Phys. **122**, 124508 (2017).
[12] Y. Chang, Y. Zhang, Y. Zhang, J. Appl. Phys. **99**, 044501 (2006).
[13] R. Yahyazadeh., A Asgari A. M Kalafi. Physica E, **33** ,77-82 (2006).
[14] A. Rashmi, S. Kranti, M. Haldar, G. Gupta et al., IEEE Trans. On Microwave Theory Tech, **51**, 607 (2003).
[15] V. Fiorentini, F. Brenardini, O. Ambacher, Appl. Phys. **80**, 1204 (2002).
[16] R. Yahyazadeh, Journal of Non - Oxide Glasses **10**(2), 57 (2018).
[17] S. Kabra, H. Kaur, S. Haldar, M. Gupta, R. S. Gupta, Solid-State Electron **52**, 25 (2008).
[18] L. Hedin, B. I. Lundqvist, J. Phys. C **4**, 2064 (1971).
[19] P. Roblin, H. Rahdin, High-speed Heterostructure Devices, Cambridge University Press, Cambridge, 277 (2002).
[20] M. A. Huque, S. A. Eliza, T. Rahman, S. K. Islam, Solid State Electronics **53**(3), 341 (2009).
[21] C. Luan, Z. Lin, Y. Lv, J. Zhao, Y. Wang, H. Chen, Z. Wang, J. Appl. Phys. **116**, 044507 (2014).
[22] M. Yang, Y. Lv, Z. Feng, W. Lin, P. Cui, Y. Liu, C. Fu, Z. Lin, J. Appl. Phys. **119**, 224501 (2016).
[23] A. F. M. Anwar, R. T. Webster, K. V. Smith, Appl. Phys. Lett. **88**, 203510 (2006).
[24] M. N. Gurusinghe, S. K. Davidsson, T. G. Andersson, Phys. Rev. B **72**(4), 045316 (2005).
[25] D. F. Brown et al, App. Phy. Lett. **3**, 042104 (2008).
[26] M. N Gurusinghe, S. K. Davidsson, T. G. Andersson, Phys. Rev. B. **72**, 045316 (2005).
[27] T. Palacios et al., IEEE Trans. Electron Devices, **52**(10), 2117 (2005).
[28] M. Yang et al., IEEE Trans. Electron Devices **63**(4), 1471 (2016).
[29] L. Hsu, W. Walukiewicz, J. Appl. Phys. **89**, 1783 (2001).
[30] T. H Yu, K. F. Brennan, J. Appl. Phys. **89**, 3827 (2001).
[31] R. Yahyazadeh, ECS Trans. **60**(1), 1051 (2014).
[32] A Kranti, Rashmi, S. Haldar, R. S. Gupta, Solid-State Electron. **46**, 621 (2002).
[33] F Stengel, S. Noor Mohammad, H Morkoc, J. Appl. Phys. **80**, 3031 (1996).
[34] P. C. Canfield, S. C. F. Lam, D. J. Allstot, IEEE J. Solid-State Circuits **25**, 299 (1990).
[35] J. C. Freeman, IEEE MTT-S Int. Microwave Symp. Dig. **3**, 2031 (2004).
[36] P. Cui, et al, Science Reports **8**, 9036 (2018).
[37] Y. F Wu, S. Keller et al., IEEE Electron Devices Lett. **18**(6), 290 (1997).